Lattice disordering in graphite under rare-gas ion irradiation studied by Raman spectroscopy

E. Asari,* I. Kamioka,* K. G. Nakamura,† T. Kawabe,* W. A. Lewis,‡ and M. Kitajima†

National Research Institute for Metals, 1-2-1 Sengen, Tsukuba-shi, Ibaraki-ken 305, Japan

(Received 26 July 1993)

We present real-time Raman measurements on graphite under 3-keV rare-gas ion irradiation. The graphite lattice disorder is estimated by the relative intensity ratio of the disorder-induced peak (~ 1360 cm^{-1}) with respect to the Raman active E_{2g2} mode peak (~ 1580 cm^{-1}), and the peak intensity ratio is found to be proportional to the square root of ion irradiation time in the beginning of ion irradiation at doses below 2.5×10^{17} ions/m^2. At the higher doses the peak intensity ratio reaches saturation. The lattice disordering rate constant steeply increases for lower mass as ion mass increases, slowly reaching a saturation value for the higher mass. Ion-mass dependence of the disordering rate is well explained by the interdefect distance model calculation.

I. INTRODUCTION

There have been many investigations on ion-irradiated graphite, since it is one of the most fascinating materials for applications to semiconductors[1] or first wall of fusion devices.[2,3] However, disordering kinetics under ion irradiation has not been well understood. We report here ion-mass effects on the lattice disordering kinetics of graphite under low-energy rare-gas ion (He^+, Ne^+, Ar^+, Kr^+, and Xe^+) irradiation studied by real-time Raman measurements.

Raman spectroscopy has been widely used for studying lattice disorder in ion-irradiated materials, such as III-V semiconductors and carbon materials, since Raman scattering is sensitive to both structural disorder and the resultant radiation damage, which normally occurs within the optical skin depth of a laser beam. Since the measurement by Smith *et al.*[4] on graphite irradiated with Ar^+, graphite irradiated with various ions has been studied by Raman spectroscopy. Raman scattering of graphite is especially sensitive to its structural disorder. While single-crystal graphite or highly oriented pyrolytic graphite (HOPG) exhibits a sharp line of Raman active E_{2g2} mode lattice vibration at ~ 1580 cm^{-1} (G peak) in the first-order Raman spectrum, disordered graphite exhibits an additional peak at ~ 1360 cm^{-1} (D peak) arising from a strong maximum in the phonon density of states. It is well known that the relative intensity ratio (R) of the D peak with respect to the G peak is inversely proportional to an inplane microcrystalline size and/or an in-plane phonon correlation length (L_a).[5–7] In addition, a broad asymmetric line at ~ 1500 cm^{-1} has been observed for a highly disordered graphite and/or an amorphous carbon. Elman *et al.*[8,9] studied Raman scattering of crystallite graphite implanted with 100 keV ^{11}B ions at a fluence in the range of 1×10^{18} to 2.5×10^{20} ions/m^2, and found that an abrupt transformation to an amorphous structure occurred at 5×10^{19} ions/m^2. The spectrum for the sample implanted at a fluence of 1×10^{18} ions/m^2 already exhibited a long-range disordered feature before the amorphization.

Using Raman spectroscopy, a surface structural change can be measured *in situ* during ion irradiation. Recently Nakamura and Kitajima[10–12] studied an early stage of ion irradiation prior to amorphization by real-time Raman measurements of HOPG samples irradiated with low-energy rare-gas ions (He^+ and Ar^+) at a flux of 3×10^{15} ions/m^2s in an ultrahigh vacuum (UHV) chamber. They showed that the peak intensity ratio R increased as irradiation time increased and it was proportional to the square root of the ion irradiation time. The results were explained in terms of reduction of the phonon correlation length using the interdefect distance (IDD) model, i.e., where the phonon correlation length is assumed to be equal to a mean distance between vacancies induced by ion irradiation. Considering damage profiles, they found that the disordering rate of the graphite lattice by Ar^+ irradiation is larger than that by He^+ irradiation. In this paper, we extended the prior study to other rare-gas ions (Ne^+, Kr^+, and Xe^+) and quantitatively investigated the ion mass dependence of the disordering rate for all rare-gas ion irradiation.

II. EXPERIMENT

The sample used was HOPG (grade ZYA; Union Carbide) with its size being $12\times12\times2$ mm^2. The sample was cleaved before each measurement by the adhesive tape technique to obtain a clean crystalline surface. Ion irradiation was performed in a UHV chamber (base pressure $<10^{-8}$ Pa) with an ion energy of 3 keV. Incident angle of the ion beam was set to be 55° from the c plane normal to avoid ion channeling. Sample current was monitored with a digital multimeter (TRS6848 ADVANTEST), and ion flux was determined via correction of the secondary electron emission. Secondary electron emission coefficients of graphite for each ion irradiation were determined experimentally using an Ag-deposited semi-

spherical cup which covers the sample and collects secondary electrons emitted from the graphite surface. Ion fluxes were 1.7×10^{15} ions/m^{2}s (high flux) and 2.7×10^{14} ions/m^{2}s (low flux). Total ion doses were below 2.6×10^{18} ions/m^2 in which graphite loss due to sputtering is negligible. Incident illumination at 514.5 nm and 500 mW was provided using a cw argon ion laser (Model INNOVA 70, Coherent). Laser annealing effects were not recognized under the present experimental conditions. Scattered radiation was collected through a sapphire window of the vacuum chamber in the backscattering configuration and analyzed by a spectrometric multichannel analyzer (SMA; D/DISA 700 Princeton Instruments Inc.). The SMA has 700 channels and detects to a width of about 400 cm^{-1}. Its gate time was set at 12 s to obtain intense signals (about 360 times the accumulation of the minimum resolution of 33 ms). Details of the experimental setup are described elsewhere.[12,13] The resultant Raman spectra were analyzed with numerical decomposition by assuming a Lorentzian line shape for all peaks.

II. RESULTS

Figure 1 shows a typical example of the first-order Raman spectra of HOPG under 3 keV Ne^+ irradiation at the low flux condition. Only the Raman active E_{2g2} mode vibration peak is observed at $\sim$1580 cm^{-1} (G) before ion irradiation [Fig. 1(a)], since HOPG has large crystalline domains. Ion irradiation has induced a peak at 1360 cm^{-1} (D) as shown in Figs. 1(b)–1(d). The solid curves are Lorentzian curve fittings and reproduce well the observed spectra. Significant peak shift was not observed for both G and D peaks. As the irradiation time increased, the peak height of the D peak increased and that of the G peak decreased. An amorphous peak was not observed at 1500 cm^{-1}. This means that ion irradiation does not cause amorphization in this ion dose region. Similar features were observed for Ne^+, Kr^+, and Xe^+ for both the high and low flux conditions.

Figure 2 shows the time dependence of observed peak intensity ratio R versus the square root of time during 3 keV Ne^+, Kr^+, and Xe^+ irradiation, where the peak intensity is the integrated area of the peak. In the low flux experiments [Figs. 2(a)–2(c)] R_{obs} increases as proportionally to the square root of the irradiation time. A slope of R_{obs} versus the square root of irradiation time decreases with increasing ion mass. In the high flux experiments [Figs. 2(d)–2(f)], R_{obs} is also proportional to the square root of irradiation time for irradiation time less than 150 s (a total dose below about 2.5×10^{17} ions/m^2). The initial increasing rate of R_{obs} for the high flux experiments is higher than that for the low flux experiments. However, for the same fluence, R_{obs} values are independent of ion flux. R_{obs} reaches saturation at around 150 s, and the saturated R_{obs} values are dependent on ion species: $\sim$0.75, $\sim$0.5, and $\sim$0.35 for Ne^+, Kr^+, and Xe^+ irradiation, respectively.

Figure 3 shows the time dependence of linewidth of the G and D peaks during 3 keV Ne^+ irradiation. The linewidths of the D peaks are larger than those of the G peaks. A slight increase in linewidth of the G peak and a drastic increase in that of the D peak were observed during irradiation. In the high flux experiment, linewidth increases rapidly from the beginning of ion irradiation and rate of increase declines at around 150 s for both the G and D peaks, which may correspond to the saturation of R. Similar behaviors of the change in linewidth were observed for Kr^+ and Xe^+ irradiation.

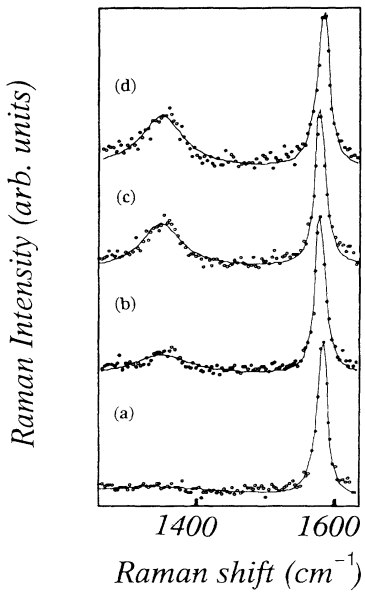

FIG. 1. First-order Raman spectra of HOPG (a) before ion irradiation, and obtained under Ne^+ irradiation after (b) 100 s, (c) 500 s, (d) 1200 s from the beginning of irradiation of 3 keV at a flux of 2.7×10^{14} ions/m^{2}s. Solid curves are the results of computer simulation.

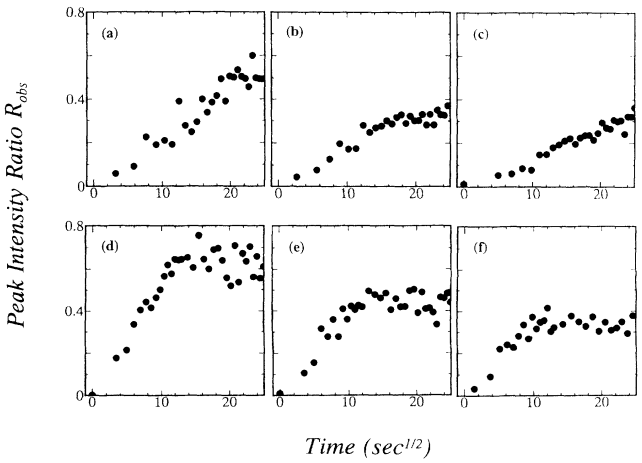

FIG. 2. Time dependence of observed peak intensity ratio R_{obs} plotted vs square root of the ion irradiation time for (a) Ne^+, (b) Kr^+, and (c) Xe^+ at a flux of 2.7×10^{14} ions/m^{2}s and for (d) Ne^+, (e) Kr^+, and (f) Xe^+ at a flux of 1.7×10^{15} ions/m^{2}s.

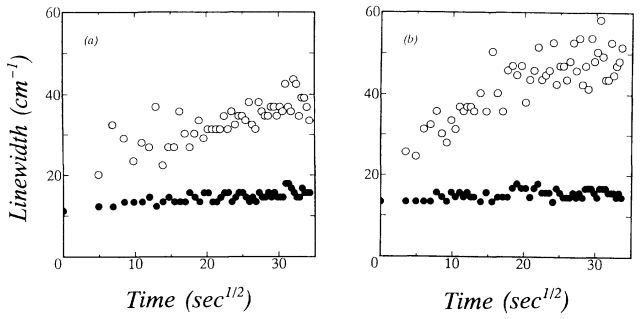

FIG. 3. Time dependence of linewidth of the $G(\bullet)$ and $D(\circ)$ peaks under 3 keV Ne^+ irradiation at ion fluxes of (a) 2.7×10^{14} ions/m^2s and (b) 1.7×10^{15} ions/m^2s.

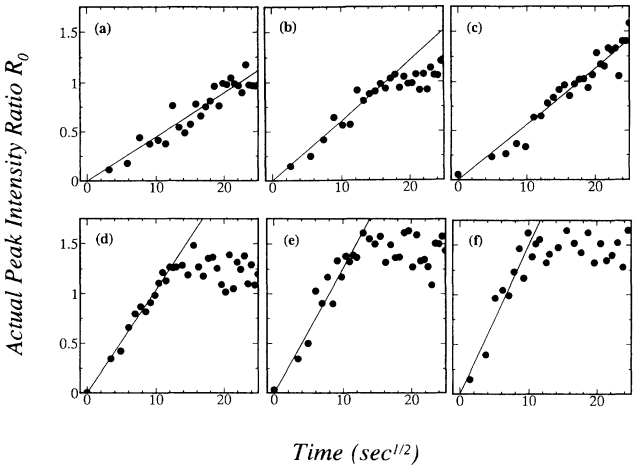

FIG. 4. Actual peak intensity ratio R_0 for (a) Ne^+, (b) Kr^+, and (c) Xe^+ at a flux of 2.7×10^{14} ions/m^2s and for (d) Ne^+, (e) Kr^+, and (f) Xe^+ at a flux of 1.7×10^{15} ions/m^2s. Solid lines are the results of least-squares calculation.

IV. DISCUSSION

Since the optical skin depth of 514.5 nm light in graphite is usually larger than an ion trajectory of ion irradiation, the observed Raman spectrum is made up of the superposition of scattering from both damaged and nondamaged layers.[11] It is then important to estimate contributions from damaged layers to study the actual ion irradiation effects. Cascade processes caused by irradiation produce a disordered region around an ion trajectory, and the Raman spectrum exhibits a double-peaked spectrum. Damaged profiles due to ion irradiation are not uniform. The damage depth distribution due to ion irradiation can be calculated using a Monte Carlo method (TRIM89 code)[14] and is well approximated by a Gaussian function. The peak position and the standard deviation of the Guassian function become smaller as the ion mass increases. The relation between the mean value of the peak intensity ratio of the D peak with respect to the G peak in the damaged region, R_0, and the observed intensity ratio, $R_{\rm obs}$, is given by

$$R_{\rm obs}=\frac{R_0 P\lambda}{8\pi m}\int_0^\infty F(x)\exp(-8\pi m x/\lambda)dx \ , \qquad (1)$$

where P is the whole range of energy deposition, m is the optical parameter (0.9 for carbon material), λ is the wave length of exciting light, x is the depth, and $F(x)$ is the normalized depth profile of the damaged layer.[10] We corrected $R_{\rm obs}$ to the mean actual relative peak intensity ratio R_0 and plotted it versus the square root of the irradiation time. Comparing $R_{\rm obs}$ (Fig. 2) and R_0 (Fig. 4), the peak intensity ratio of the damaged area is much larger than the observed one. The slope of R_0 is smaller in the Ne^+ case than in the Kr^+ and Xe^+ cases.

Tuinstra and Koenig[5] obtained an empirical relation $R=C/L_a$, where L_a is the in-plane microcrystallite size in graphite and C is 4.4 nm. L_a is considered to correspond to the in-plane phonon correlation length. An increase in R means an increase in the D peak and a decrease in the micryocrystallite size or phonon correlation length in the graphite plane.[7] We adopt here the IDD model[10,11] which describes well the time dependence of R for He^+ and Ar^+ irradiation. In the IDD model it is assumed that the in-plane phonon correlation length is equal to the mean distance (L) between vacancies in the graphite plane induced by ion irradiation. The increase in the D peak is explained by a contribution from the maximum of the phonon density of states due to relaxation of wave vector selection rule. The defects cause a confinement of phonon correlation and a relaxation of the wave vector selection rule (see Appendix A).

In general, the mean number of vacancies (N_L) per unit area in a graphite layer in the ion penetration range is calculated by

$$N_L=Nf\sigma\nu\varphi t \ , \qquad (2)$$

where N is the density of target (1.25×10^{29} atoms/m^3 for graphite), f is the distance between graphite layers (0.335 nm), σ is the displacement cross section, φ is the incident ion flux, ν is the mean number of displaced atoms in the cascade per primary knock-on, and t is the irradiation time. Both σ and ν depend on ion mass and ion energy (see Appendix B). The mean actual relative intensity ratio is expressed, based on the IDD model, by

$$R=C(Nf\sigma\nu)^{1/2}(\varphi t)^{1/2}=\alpha_{\rm calc}(\varphi t)^{1/2} \ , \qquad (3)$$

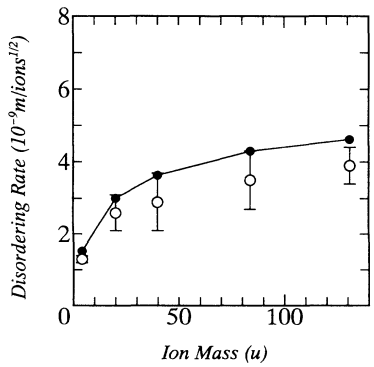

FIG. 5. Ion mass number dependence of disordering rate: $(\circ)$ experimental value, $(\bullet)$: calculated value by Eq. (3).

TABLE I. Calculated displacement cross sections, damage functions, and disordering rate constants obtained by experiments and interdefect distance model calculation for He^+, Ne^+, Ar^+, Kr^+, and Xe^+.

Ion	ν	σ (10^{-21} m^2)	α_{obs} (10^{-9} m/ions$^{1/2}$)	α_{calc} (10^{-9} m/ions$^{1/2}$)
He^+	2.32	1.25	1.3±0.1	1.53
Ne^+	2.43	4.59	2.6±0.3	3.01
Ar^+	2.29	7.12	2.9±0.8	3.64
Kr^+	2.05	11.1	3.8±0.5	4.30
Xe^+	1.87	14.1	4.1±0.6	4.62

where α_{calc} is the disordering rate constant. An experimental value α_{obs} of the disordering rate constant is also estimated from the gradient of R_0 to ion dose. Figure 5 shows a comparison of α_{calc} and α_{obs} plotted versus ion mass. In the low mass region, experimental values of the lattice disordering rate increased steeply as the ion mass increased, slowly reaching a saturation value in the high mass region. The calculation reproduces this tendency and the values are consistent with experimental values. All parameters used for the calculation and experimentally obtained values are listed in Table I.

R_0 increased proportionally with the square root of the irradiation time until ~150 s [Figs. 4(d)–4(f)], and after that time it approached saturation values being about 1.25, 1.3, 1.4, and 1.5 for Ne^+, Ar^+, Kr^+, and Xe^+ irradiation, respectively. Table II shows the critical ion dose at which R_0 starts to deviate from its square root relation to the irradiation time. The critical ion dose is $\sim 2.5\times10^{17}$ ions/m^2, and the doses for Ne^+ irradiation are larger than for Ar^+, Kr^+, and Xe^+ irradiation. The corresponding critical defect density estimated by Eq. (2) increases as the ion mass increases (Table II). There are two possible reasons for the saturation of R_0: (1) creation of vacancy clusters and (2) breakdown of the relation between the peak intensity ratio and the phonon correlation length. At high ion doses, the vacancy density becomes so high, and the vacancies aggregate together. When vacancies aggregate and create clusters, the effective distance between the vacancies increases. The empirical relation between the peak intensity ratio and the phonon correlation length has been established only for large L_a.[5,6] Since the D peak comes from a maximum of the phonon density of states due to relaxation of the wave vector selection rule, the peak intensity ratio should approach a finite value for very small L_a.

In conclusion, real-time Raman measurements have been performed on graphite under 3 keV rare-gas-ion irradiation. The peak intensity ratio was proportional to the square root of the ion irradiation time in the beginning of ion irradiation for doses below 2.5×10^{17} ions/m^2. The disordering rate constant increases as ion mass increased. The ion mass effect on the disordering rate is well explained by the interdefect distance model calculation.

TABLE II. Critical ion dose at which R_0 starts to deviate from the square root relation to the irradiation time and the critical vacancy density.

Ion	Ion dose (10^{17} ions/m^2)	Vacancy density (10^{17} vacancies/m^2)
Ne^+	2.6±0.4	1.21±0.19
Ar^+	2.0±0.5	1.36±0.34
Kr^+	2.1±0.4	2.00±0.38
Xe^+	2.1±0.4	2.32±0.54

APPENDIX A: RELAXATION OF WAVE VECTOR SELECTION RULE

Here we show the relaxation of the wave vector selection rule in graphite which includes defects, based on the spatial correlation model.[15–17] The wave function of a phonon with wave vector $\mathbf{k}_0$ in an infinite crystal is expressed with the plane wave

$$\phi(\mathbf{k}_0,\mathbf{r})=u(\mathbf{k}_0,\mathbf{r})\exp(-i\mathbf{k}_0\cdot\mathbf{r}) , \tag{A1}$$

where $u(\mathbf{k}_0,\mathbf{r})$ has a periodicity of the lattice. In a crystal which includes a small number of defects, the phonon plane wave is scattered by the defects. If we assume an attenuation probability ($\mathbf{W}$) of a phonon with wave vector $\mathbf{k}_0$ and propagation direction of $\mathbf{r}$ in a single collision, the intensity of the phonon wave after n collisions with defects is $\mathbf{W}^n$. When we consider that the distribution of defects is uniform and that the separation of defects in the $\mathbf{r}$ direction is L, the number of collisions of the phonon wave ($\mathbf{k}_0$) over a distance r is r/L. The wave function of a phonon in a crystal with defects is expressed as

$$\begin{aligned}\psi(\mathbf{k}_0,\mathbf{r})&=\exp\left[\frac{-r}{L}\ln(1/W)\right]u(\mathbf{k}_0,\mathbf{r})\exp(-i\mathbf{k}_0\cdot\mathbf{r})\\&=\psi'(\mathbf{k}_0,\mathbf{r})u(\mathbf{k}_0,\mathbf{r})\end{aligned} \tag{A2}$$

This corresponds to the attenuation of the phonon wave by defects. The wave function ψ' might be expanded in a Fourier series:

$$\psi'(\mathbf{k}_0,\mathbf{r})=\int C(\mathbf{k}_0,\mathbf{k})\exp(-i\mathbf{k}\cdot\mathbf{r})d^3\mathbf{k} , \tag{A3}$$

where the Fourier coefficients $C(\mathbf{k}_0,\mathbf{k})$ are given by

$$C(\mathbf{k}_0,\mathbf{k})=\frac{1}{(2\pi)^3}\int\psi'(\mathbf{k}_0,\mathbf{r})\exp(i\mathbf{k}\cdot\mathbf{r})d^3\mathbf{r} . \tag{A4}$$

Inserting ψ' from Eq. (A2) into Eq. (A4) yields

$$C(\mathbf{k}_0,\mathbf{k})=\frac{1}{(2\pi)^3}\frac{\Gamma}{1+\Gamma^2(\mathbf{k}-\mathbf{k}_0)^2} , \tag{A5}$$

where

$$\Gamma=\frac{L}{\ln(1/W)} . \tag{A6}$$

Thus ψ' is the superposition of eigenfunctions with $\mathbf{k}$ vectors with Lorentzian distribution with width of $2/\Gamma$ centered at $\mathbf{k}_0$. The phonon transition matrix elements $|\langle \mathbf{k}_0|\hat{O}|\mathbf{k}\rangle|^2$ have nonvanishing values also for $\mathbf{k}\neq\mathbf{k}_0$ according to

$$|\langle \mathbf{k}_0|\hat{O}|\mathbf{k}\rangle|^2=|\langle \mathbf{k}_0|\hat{O}|\mathbf{k}_0\rangle|^2 C(\mathbf{k},\mathbf{k}_0)^2 , \tag{A7}$$

where $\hat{O}$ is the photon-phonon interaction operator. The attenuation of the phonon is in effect a relaxation of the $\Delta\mathbf{k}=0$ selection rule. Using the relaxation of the wave vector conservation rule, the one phonon Raman spectrum is expressed by

$$I(\omega)\propto \sum_{k} C(\mathbf{k}_0,\mathbf{k})^2 g[\omega_0(\mathbf{k})]\frac{\Lambda}{1+\Lambda^2[\omega-\omega_0(\mathbf{k})]^2} , \tag{A8}$$

where Λ is the linewidth of each transition and $g[\omega(\mathbf{k})]$ is the phonon density of states. Since the phonon density of states[18] has a maximum at ~ 1360 cm^{-1}, the Raman spectrum of graphite with defects shows the D peak.

APPENDIX B: DISPLACEMENT CROSS SECTION

The displacement cross section is calculated by the Sigmund theory[19,20] by

$$\sigma=1.9635a^2(m_1/m_2)^{1/3}(2z_1z_2e^2/a)^{2/3} \times E_0^{-1/3}(E_d^{-1/3}-T_{\max}^{-1/3}) , \tag{B1}$$

where a is the screening radius, E_0 the incident ion energy, $T_{\max}$ the maximum of the transferred energy, e the electronic charge, E_d the threshold energy for displacement, and m_1, z_1, m_2, and z_2 the masses and atomic number of the projectile and target, respectively. The E_d is determined to be 29.7 eV by the etch-decoration technique.[21] $T_{\max}$ is given by

$$T_{\max}=4m_1m_2E_0/(m_1+m_2)^2 . \tag{B2}$$

The mean number of displaced atoms in the cascade per primary knock-on ν can be calculated by a simplified model of the Kinchin-Pease theory,[22]

$$\nu=0.5[1+\ln(T_{\max}/2E_d)] . \tag{B3}$$

Then both σ and ν values are dependent on the incident ion energy E_0 and the ion mass m_1.

---

*Also at the University of Tsukuba.
†Authors to whom correspondence should be addressed.
‡Also at Stanford University, Stanford, CA 94305.

[1]M. S. Dresselhaus and G. Dresselhaus, in *Light Scattering in Solid III,* edited by M. Cardona and G. Guntherodt (Springer-Verlag, Berlin, 1982), p. 2.
[2]M. Kitajima, K. Aoki, and M. Okada, J. Nucl. Mater. **149**, 269 (1987).
[3]T. Tanabe, S. Muto, Y. Gotoh, and K. Niwase, J. Nucl. Mater. **175**, 258 (1990).
[4]J. E. Smith, Jr., M. H. Mrodzky, B. L. Crowder, and M. I. Nathan, J. Non-Cryst. Solids **8-10**, 179 (1972).
[5]F. Tuinstra and J. L. Koenig, J. Chem. Phys. **53**, 1126 (1970).
[6]D. S. Knight and W. B. White, J. Mater. Res. **4**, 285 (1989).
[7]K. Nakamura, M. Fujitsuka, and M. Kitajima, Phys. Rev. B **41**, 12 260 (1990).
[8]B. S. Elman, M. S. Dresselhaus, G. Dresselhaus, E. W. Maby, and H. Mazurek, Phys. Rev. B **24**, 1027 (1981).
[9]B. S. Elman, M. Shayegan, M. S. Dresselhaus, H. Mazurek, and G. Dresselhaus, Phys. Rev. B **25**, 4142 (1982).
[10]K. Nakamura and M. Kitajima, Phys. Rev. B **45**, 5672 (1992).
[11]K. Nakamura and M. Kitajima, Phys. Rev. B **45**, 78 (1992).
[12]K. Nakamura and M. Kitajima, Appl. Phys. Lett. **59**, 1550 (1991).
[13]E. Asari, K. G. Nakamura, M. Kitajima, and T. Kawabe, Phys. Rev. B **47**, 11 143 (1993).
[14]J. F. Ziegler, J. P. Biersack, and U. Littmark, in *The Stopping and Range of Ions in Solids* (Pergamon, New York, 1985), p. 109.
[15]H. Richter, Z. P. Wang, and L. Ley, Solid State Commun. **39**, 625 (1981).
[16]R. J. Nemanich and S. A. Solin, Phys. Rev. B **20**, 392 (1970).
[17]P. Lespade, R. Al-Jishi, and M. S. Dresselhaus, Carbon **20**, 427 (1982).
[18]M. Maeda, Y. Kuramoto, and C. Horie, J. Phys. Soc. Jpn. **47**, 337 (1979).
[19]P. D. Townsend, J. C. Kelly, and N. E. W. Hartley, in *Ion Implantation, Sputtering and their Applications* (Academic, London, 1976), p. 177.
[20]P. Sigmund, in *Sputtering by Particle Bombardment I,* edited by R. Behrisch (Springer-Verlag, Berlin, 1981), p. 9.
[21]G. L. Montet, Carbon **11**, 89 (1973).
[22]G. H. Kinchin and R. S. Pease, Rep. Prog. Phys. **18**, 1 (1955).